AD734410

MTI . . . research and development division

42

Unclassified

Security Classification

DOCUMENT CONTROL DATA - R & D

(Security classification of title, body of abstract and indexing annotation must be entered when the overall report is classified)

1. ORIGINATING ACTIVITY *(Corporate author)* Mechanical Technology Incorporated 968 Albany-Shaker Road Latham, New York 12110	2a. REPORT SECURITY CLASSIFICATION Unclassified 2b. GROUP N/A

3. REPORT TITLE

A Brief Comparison of the Accuracy of Time-Dependent Integration Schemes for the Reynolds Equation

4. DESCRIPTIVE NOTES *(Type of report and inclusive dates)*

Technical Report

5. AUTHOR(S) *(First name, middle initial, last name)*

Richard L. Coleman

6. REPORT DATE	7a. TOTAL NO. OF PAGES	7b. NO. OF REFS
September, 1971	32	6

8a. CONTRACT OR GRANT NO. N00014-70-C-0135 b. PROJECT NO. c. d.	9a. ORIGINATOR'S REPORT NUMBER(S) 71TR59 9b. OTHER REPORT NO(S) *(Any other numbers that may be assigned this report)* None

10. DISTRIBUTION STATEMENT

This Document has been approved for public release and sale; its distribution is unlimited.

11. SUPPLEMENTARY NOTES	12. SPONSORING MILITARY ACTIVITY
None	Office of Naval Research

13. ABSTRACT

Two dynamic methods are compared for integrating the Reynolds equation as applied to determining the axial dynamics of a spool bearing. It is shown that very sensitive phase shifts in the numerical schemes can badly falsify the dynamics; therefore, care is needed in interpreting results using classical methods. Second order temporal accuracy can alliviate these problems; one such scheme is presented with excellent phase properties that is just as computationally efficient per time step as any of the first order accurate schemes.

MTI-71TR59

A Brief Comparison of the Accuracy of Time-Dependent Integration Schemes For the Reynolds Equation

Prepared for
Office of Naval Research

September 1971

MECHANICAL TECHNOLOGY INCORPORATED
968 Albany-Shaker Road
Latham, New York 12110

NO. 71TR59

DATE: September, 1971

TECHNICAL REPORT

A Brief Comparison of the Accuracy of Time-Dependent
Integration Schemes for the Reynolds Equation

by

Richard L. Coleman

R. L. Coleman / C.P.

Author (s)

Coda H. T. Pan

Approved

Approved

Prepared for

Office of Naval Research

Prepared under

N00014-70-C-0135

MTI
MECHANICAL TECHNOLOGY INCORPORATED

968 ALBANY - SHAKER ROAD — LATHAM, NEW YORK — PHONE 785-0922

MTI-2310-65)

ABSTRACT

Two dynamic methods are compared for integrating the Reynolds equation as applied to determining the axial dynamics of a spool bearing. It is shown that very sensitive phase shifts in the numerical schemes can badly falsify the dynamics and thus care is neede in interpreting results using classical methods. Second order temporal accuracy can alleviate these problems and one such scheme is presented with excellent phase properties that is just as computationally efficient per time step as any of the first order accurate schemes.

TABLE OF CONTENTS

Introduction

A large number of papers have appeared in the gas bearing literature solving the time dependent compressible Reynolds equation by direct numerical integration. A typical example of modern practice is given in [1]. In some of our recent work a notable example of the sensitivity of time transient dynamics to the accuracy of the integration scheme appeared. The most important result was the failure of the classical implicit scheme to adequately track the system dynamics except when the time step was very small. It will be shown that this defect is due to phase shifts in the numerical solution and that these problems can be adequately cured by using an extrapolated Crank-Nicolson scheme.

Such phase shifts can have catastrophic effects in the numerical simulation; however, they are dependent on the particular integration scheme used. The fact that a scheme is inherently $O(\Delta T)$ in itself is a priori insufficient to categroize the scheme as having poor phase properties. For example, in the classical work [2] the infinite length journal bearing was solved using PH as the dependent variable (a natural choice). In some of our own unpublished work, the calculations of [2] are corroborated; further, however, both the schemes discussed here are used (solving for PH), and phase shifts are highly mollified, although the extrapolated Crank-Nicolson schemes proves itself the superior. In diverse applications such as [1], careful a posteriori testing is necessary to validate the system behavior extracted from the numerics.

The problem of interest was to solve for the axial dynamics of a spool bearing with spiral groove thrust plates and herringbone groove journal (See [3], Figures 1 and 2). With no radial eccentricity, the geometry is axisymmetric, and thus spatially the problem is one dimensional. Appendix 1 depicts the equations of interest according to the narrow groove theory and Appendix 2 derives the equations of motion for the axial dynamics.

Implicit Scheme and Results

In Appendix 3 the basic spatial discretization for the divergence form of Reynolds equation is derived. The implicit scheme approximates the highest spatial derivatives at the advanced time level. All other terms are evaluated at the current time level. Thus (33) takes the form

$$a^n_{J+.5} \Delta_J P^{n+1} - b^n_{J+.5} - a^n_{J-.5} \Delta_{J-1} P^{n+1} + b^n_{J-.5}$$

$$= .5 \left(\Delta S_J \, g^n_{J+} + \Delta S_{J-1} \, g^n_{J-} \right) \frac{P^{n+1}_J - P^n_J}{\Delta T} + .5 \left(\Delta S_J \, c^n_J + \Delta S_{J-1} \, c^n_{J-} \right) \tag{1}$$

$$+ \Lambda \frac{c_o}{r_o} \frac{2\nu}{\omega_1 + \omega_2} R_j \bar{C}_h \left(P^n_J \left[\partial H^n_{r,J+}/\partial T + \partial H^n_{r,J-}/\partial T \right] + \bar{C}_h \frac{P^{n+1}_J - P^n_J}{\Delta T} \right)$$

where superscript n refers to current time level, and n+1 the advanced time level. As discussed in Appendix 3, the last term on the right only appears at the chamfer and if there is no chamfer $\bar{C}_h = 0$.

The equations of motion (28) given in Appendix 2 are integrated by a standard Euler scheme accurate to $O(\Delta T)$, which is consistent with (1); thus

$$(\bar{\varepsilon}_1^{n+1} - \bar{\varepsilon}_1^{n})/\Delta T = \bar{\varepsilon}_2^{n}$$

$$(\bar{\varepsilon}_2^{n+1} - \bar{\varepsilon}_2^{n})/\Delta T = (-a_e^n + F^n/m)/c_o\nu^2 \tag{2}$$

(1) and (2) can be computed independently in parallel to obtain the new pressure P^{n+1} and the new eccentricity $\bar{\varepsilon}_1^{n+1}$. The new gap is then

$$H_{r\pm}^{n+1} = 1 \mp \bar{\varepsilon}_1^{n+1} \tag{3}$$

and the gas bearing force at the advanced time is obtained by integrating P^{n+1}.

There are many allowable variants of (1); e.g., evaluating b at n+1 instead of n, but these are still $O(\Delta T)$. The choice of (1) as the implicit variant is dictated by the ellipticity of (20) which implies the tridiagonal matrix to be inverted to solve (1) is diagonally dominant, and therefore Gaussian elimination without pivoting is stable, so (1) can be very efficiently solved (see the discussion in Appendix A of [4]).

The spool bearing with the geometry given in Appendix 4 was tested for stability using the implicit scheme (1) and (2). The gap was given an initial perturbation of approximately 1.13 in./sec. Time was nondimensionalized by letting ν = 400 Hertz, and the natural frequency of this particular bearing is about 6400 Hertz. In Figure 1 the nondimensional eccentricity versus nondimensional time is shown for three different time steps. The abscissa is shown in a new nondimensional time $T' = T/(2\pi/288)$, the ordinate is the negative of the nondimensional eccentricity, and N^* corresponds very closely to the number of time steps per cycle of natural frequency.

The clear picture that emerges from Figure 1 is the large variation of bearing response as a function of time step, and even as Figure 2 shows with $N^* = 144$, the bearing appears to be neutrally stable. It can be shown that this bearing should be stable, so that the case $N^* = 144$ still depicts the dynamics incorrectly. Such a posteriori examination of the data shows the time step must be much smaller yet to obtain correct results.

A slightly deeper investigation explains the apparent instability shown in Figure 1. Let us consider the bearing response to a forced-gap oscillation. The equations of motion are uncoupled, and the bearing gap is forced by

$$H = 1 + \tilde{\varepsilon} \cos(T) \tag{4}$$

where ε generally is very small (in this case $\tilde{\varepsilon} = .01$). The bearing force is decomposed into a Fourier series over one cycle

$$F(T) = a_o + \sum_{i=1}^{\infty} \left\{ a_i \cos(iT) + b_i \sin(iT) \right\} \tag{5}$$

Eventually the force F will entrain itself into a periodic function, so the coefficients $\{a_i\}$ and $\{b_i\}$ will not change from cycle to cycle. In fact, with $\tilde{\varepsilon}$ small, only a_1 and b_1 are nonzero. By the usual conventions, dimensionally the in-phase and out-of-phase components of the bearing stiffness are $U = -a_1/\bar{\epsilon}c_0$ and $V = b_1/\bar{\epsilon}c_0$ respectively. Table 1 shows the results for ν= 400 Hertz, for N* taking on the same values as in Figure 1. The two columns under $O(\Delta T)$ show the in-phase and out-of-phase components for this implicit scheme. U and V are in units of lb/in.

TABLE 1. U and V for ν= 400

	$O(\Delta T)$		$O(\Delta T^2)$	
N*	U	V	U	V
18	389,767	-134,424	440,680	-42,782
36	414,829	- 89,517	437,861	-41,074
72	426,269	- 65,556	---	---
X	437,709	- 41,595	436,921	-40,504
LINEAR	438,521	- 39,810	438,521	-39,810

The row marked LINEAR shows the results obtained from a small perturbation analysis. The major source of error is the large shifts in V as a function of N*. It is interesting to note that both U and V are very linear functions of ΔT (equivalently 1/N*). The row marked X is the result of extrapolating the N* = 36 and N* = 72 solutions to infinity to yield a solution of accuracy $O(\Delta T^2)$. It is more descriptive to recast F in the form

$$F = K\cos(T-\phi)\ (-\bar{\epsilon}c_o)$$

where $K = (U^2 + V^2)^{1/2}$ and $\phi = \arctan(-V/U)$. These results are shown in Table 2 with ϕ actually given in degrees and not radians.

TABLE 2. K and ϕ for ν = 400 Hertz

	$O(\Delta T)$		$O(\Delta T^2)$	
N*	K	ϕ	K	ϕ
18	412,296	19.03	442,752	5.54
36	424,378	12.18	439,783	5.36
72	431,280	8.74	--	--
X	439,681	5.43	438,794	5.30
LINEAR	440,324	5.18	440,324	5.19

The major source of error can now be seen to be in the phase lag ϕ, and just a few degrees shift cause large errors in V. The implicit scheme induces excessive phase lag in the numerical solution. In order to see why the excessively poor bearing stability properties of Figure 1 arise consider Table 3 which is similar to Table 1, but ν = 7000 Hertz.

TABLE 3. U and V for ν= 7000 Hertz

	$O(\Delta T)$		$O(\Delta T^2)$	
N*	U	V	U	V
18	468,700	-56,042	476,473	30,766
36	472,580	-12,076	474,425	31,519
72	473,508	9,699	--	--
X	474,436	31,474	473,742	31,770
LINEAR	477,575	34,314	477,575	34,314

The same comments apply here as apply to Table 1. For $N^* = 18$ and 36 case V shows a lagging phase rather than the leading phase of the actual solution. Again it is important to recognize that V can be very accurately described by $V = V_0 + V_1/N^*$, and it is the excessive size of V_1, a characteristic of this implicit scheme, that degrades the results. From Table 1 and Table 3 we are able to infer that this scheme causes a large shift in the negative direction of V.

For one degree of freedom systems the solution of the characteristic polynomial is given by

$$\begin{aligned} m\nu^2 &= U(\nu) \\ V(\nu) &= 0. \end{aligned} \tag{7}$$

If U and V are obtained numerically as a function of N^*, then $U = U(\nu, N^*)$ and $V = V(\nu, N^*)$. In the above example, $V(\nu, N^*)$ is approximately invariant with N^* and always $U(\nu, N^*) > 0$. $V(\nu, N^*)$ shows large shifts in the negative direction as N^* goes to 0. The zero crossing occurs at larger values of ν(V has monotone increasing behavior as a function of ν for this bearing away from $\nu = 0$). Since U is approximately invariant with N^*, by (7) m, the critical mass, must get small with N^*. Thus, the bearing has a small apparent critical mass, which explains the instability apparent in Figure 1 (which worsens with smaller N^*).

Second Order Scheme and Comparisons

It will now be shown how an extrapolated Crank-Nicolson scheme cures the preceding defects with no essential penalty in computing time. The efficiency of this scheme was shown in [4]. Define

$$P^{n+.5} = 1.5P^{n} - .5P^{n-1} \tag{8}$$

The extrapolated Crank-Nicolson scheme is

$$a_{J+.5}^{n+.5}\,\Delta_J\left[.5(P^{n+1}+P^{n})\right] - b_{J+.5}^{n+.5} - a_{J-.5}^{n+.5}\,\Delta_{J-1}\left[.5(P^{n+1}+P^{n})\right] + b_{J-.5}^{n+.5}$$

$$= .5\left(\Delta S_J g_{J+}^{n+.5} + \Delta S_{J-1} g_{J-}^{n+.5}\right)\frac{P_J^{n+1}-P_J^{n}}{\Delta T} + .5\left(\Delta S_J c_{J+}^{n+.5} + \Delta S_{J-1} c_{J-}^{n+.5}\right) \tag{9}$$

$$+ \Lambda\frac{c_o}{r_o}\,\frac{2\nu}{\omega_1+\omega_2}\,R_j\bar{C}_h\left(P_J^{n+.5}\left[\partial H_{r,J+}^{n+.5}/\partial T + \partial H_{r,J-}^{n+.5}/\partial T\right] + \bar{C}_h\,\frac{P_J^{n+1}-P_J^{n}}{\Delta T}\right).$$

Again the last term on the right appears only at the chamfer. In any coefficient evaluated at n + .5, P is obtained from (8). $H_r^{n+.5}$ for these coefficients is determined as shown below. Note that (8) cannot be used at the initial value of time or whenever there is a discontinuity in the equations of motion as a function of time. Whenever this occurs (1) is used with ΔT changed to $.5\Delta T$. Since (9) is a linear system for P^{n+1}, it is no more time consuming to solve than (1).

The equations of motion cannot be integrated in the same fashion as in (2). A modified Euler integration is used to maintain an $O(\Delta T^2)$ accuracy. This is a two step integration with the first step given by (2) with ΔT replaced by $.5\Delta T$.

$$(\bar{\epsilon}_1^{n+.5} - \bar{\epsilon}_1^{n})/.5\Delta T = \bar{\epsilon}_2^{n}$$

$$(\bar{\epsilon}_2^{n+.5} - \bar{\epsilon}_2^{n})/.5\Delta T = (-a_e^n + F^n/m)/c_o\nu^2 \tag{10}$$

To integrate to the full step it is necessary to obtain the gas bearing force F at T + $.5\Delta T$. This is accomplished by integrating $P^{n+.5}$ given by (8). The second step in the integration is

$$(\bar{\epsilon}_1^{n+1} - \bar{\epsilon}_1^{n})/\Delta T = \bar{\epsilon}_2^{n+.5}$$

$$(\bar{\epsilon}_2^{n+1} - \bar{\epsilon}_2^{n})/\Delta T = (-a_e^{n+.5} + F^{n+.5}/m)/c_o\nu^2 \tag{11}$$

which is centered about n + .5. Now analogous to (3),

$$H_{r\pm}^{n+.5} = 1 \mp .5\,(\bar{\epsilon}_1^{n} + \bar{\epsilon}_1^{n+1}). \tag{12}$$

The same calculation shown in Figure 1 for N*=18 is depicted in Figure 3. If N* is repeatedly doubled there is negligible shift in the results. Further contrast in the quality can be seen in the tables. Under the heading $O(\Delta T^2)$ are listed the results for this scheme. The row marked X is a quadratic extrapolation yielding an $O(\Delta T^3)$ error. The

$N^* = 18$ solution is better than any of the implicit cases shown, and from Table 2 it can be seen there is negligible phase shift. Table 3 indicates both U and V are accurate at the higher frequencies, and thus from Tables 1 and 3 there is no shift in V as illustrated for the implicit scheme. This explains the very good results depcited in Figure 3.

It is interesting to note in the tables the slight systematic differences between the extrapolated solutions and the small perturbation analysis. The perturbation results were obtained from another program in which the difference approximations were derived in a slightly different fashion. Consistent use of the same difference approximations would yield identical results.

Discussion and Conclusions

The proven convenience of dynamic simulation programsto validate bearing designs makes these programs valuable tools. We have illustrated one of the difficulties that require careful consideration in interpreting stability results, for example, in complicated dynamic simulations. Very fortunately simple a posteriori comparisons can elucidate whether numerical difficulties exist (although not necessarily cure them).

It was shown that the classical implicit scheme with an $O(\Delta T)$ truncation error, because of the size of that truncation error, will manifest slight phase shifts in the numerical solution which will appear as errors particularly in the out-of-phase component of the bearing force. This results in falsification of the stability behavior of the bearing. An extrapolated Crank-Nicolson scheme with $O(\Delta T^2)$ truncation error cures these difficulties and has excellent phase properties.

What was not considered was the determination of optimal $O(\Delta T)$ schemes which minimize particularly phase errors. Thus, the possibility is not ruled out that variants of an implicit scheme will have much better phase properties, however, it is unlikely that such schemes can match the excellent accuracy of the linear $O(\Delta T^2)$ scheme demonstrated here.

Changing bearing parameters is not expected to make significant changes in the results. When Λ was reduced by a factor of five by changing p_a, the same very poor out-of-phase characteristics depicted in Table 1 resulted.

In general, if testing of a classical scheme indicates numerical difficulties (albeit numerical stability or truncation error effects), then a simple alteration to an extrapolated Crank-Nicolson scheme can cure both problems without essential penalty in computation time.

Acknowledgements

The basic part of the theoretical work in this paper was supported under contracts N00030-66-C-0189 and N00030-71-C-0105, Subcontract No. 413, Purchase Order IL-H-307229-2, with the C. S. Draper Laboratory of the Massachusetts Institute of Technology. More extensive stability results are given in the appendix of the report [6] which, however, has limited circulation. Further theoretical developments and numerical comparisons were supported by the Office of Naval Research under contract N00014-70-C-0135 administered by Mr. Stanley Doroff.

The author wishes to thank Dr. C. H. T. Pan for many discussions on a variety of technical points.

REFERENCES

1. W. Shapiro and R. Colsher, "Implementation of Time Transient and Step-Jump Dynamic Analyses of Gas-Lubricated Bearings", Journal of Lubrication Technology, Trans. ASME, Series F, Vol. 92, 1970, pp. 518-529.

2. V. Castelli and H. G. Elrod, "Solution of the Stability Problem for 360 Deg Self-Acting, Gas-Lubricated Bearings", Journal of Basic Engineering, Trans, ASME, Series D, Vol. 87, 1965, pp. 199-212.

3. W. G. Denhard and C. H. T. Pan, "Application of Gas-Lubricated Bearings to Instruments", Journal of Lubrication Technology, Trans. ASME, Series F, Vol. 90, 1968, pp. 731-740.

4. R. L. Coleman, "Economic Difference Methods of High Accuracy for Solution of the Time-Dependent, Gas-Lubrication Equation", Report R-629, Instrumentation Laboratory, MIT, Cambridge, Mass., November 1968.

5. J. H. Vohr and C. H. T. Pan, "Design Data of Gas Lubricated Spin Axis Bearings for Gyroscopes", Report MTI-68TR29, Mechanical Technology Inc., Latham, New York, June 1968.

6. R. L. Coleman, "Design of High Performance Gas-Lubricated Spin Axis Bearings", Report MTI-71TR12, Mechanical Technology Inc., Latham, New York, February 1971.

APPENDIX 1. Equations and Boundary Conditions

The purpose of this appendix is to display the particular one dimensional parabolic equation being solved along with the appropriate boundary conditions. We are interested in the pressure profile in a spool bearing with no radial eccentricity where the thrust plates are spiral grooved and the journal bearing herringbone grooved.

It has been shown [5] that according to the narrow groove theory the one dimensional Reynolds equation in generalized coordinates for all spiral groove geometries in nondimensional form is

$$-\frac{\partial \Psi_S}{\partial S} - \Lambda \frac{2\nu}{\omega_1 + \omega_2} \frac{\partial}{\partial T} (RK_\omega PH_r) = 0 \tag{13}$$

where the mass flux is

$$\Psi_S = -PH_r^3 K_1 R \frac{\partial P}{\partial S} + \Lambda_\delta K_4 R^2 \cos\beta \; P \tag{14}$$

with

$$\begin{aligned}
\Lambda &= \frac{6\mu}{p_a}\left(\frac{r_o}{c_o}\right)^2 (\omega_1 + \omega_2) \\
\Lambda_\delta &= \Lambda \frac{\omega_2 - \omega_1}{\omega_2 + \omega_1} \alpha(1-\alpha) \sin\beta \frac{\delta}{c} \\
K_\omega &= \alpha\Gamma + 1 - \alpha \\
K_1 &= [\alpha(1-\alpha)\sin^2\beta \; (\Gamma^3 - 1)^2 + \Gamma^3] / [(1-\alpha)\Gamma^3 + \alpha] \\
K_4 &= [\Gamma^3 - 1]/[(1-\alpha)\Gamma^3 + \alpha] \\
T &= \nu t \\
S &= s/r_o \\
P &= p/p_a \\
H_r &= h_r/c_o
\end{aligned} \tag{15}$$

The function R(S) is the normalized bearing radius at S; if r_j is the radius of the journal bearing, then $R(S) = r_j/r_o$ for all S located along the journal.

All other parameters are conventional spiral groove quantities and are defined in the nomenclature and in [5].

Let us now consider the boundary conditions. At the ambient edges of the thrust plates P = 1. A chamfer region may exist between the thrust plates and the journal bearing. Two possible boundary conditions are allowed at the chamfer - it may be vented to some arbitrary pressure P_c which need not be $P_c = 1$, or if unvented then it can be shown [5 , p. 28] that

$$\Psi_S\Big|_{in} - \Psi_S\Big|_{out} = \frac{6\mu}{\pi p_a^2 c_o^3} \frac{\partial}{\partial t} (pV_c). \tag{16}$$

where V_c = chamfer volume. If the chamfer cross section is shaped as an isosceles triangle with height c_h and base $2c_h$, then the approximate chamfer volume is $2\pi r_j c_h^2$, however a better approximation is

$$V_c = 2\pi r j c_h (c_h + h_t) \tag{17}$$

where h_t = thrust plate gap at the chamfer. (17) includes the chamfer volume contribution from the thrust plate gap which is only important when axial time dependent effects are being considered. Using (17), (16) may now be rewritten

$$\Psi_S\Big|_{in} - \Psi_S\Big|_{out} = \Lambda \frac{c_o}{r_c} \frac{2\nu}{\omega_1 + \omega_2} R_j \bar{C}_h \left[P \frac{\partial Hr}{\partial T} + \bar{C}_h \frac{\partial P}{\partial T} \right] \tag{18}$$

where $\bar{C}_h = c_h/c_o$ and $R_j = r_j/r_o$. If $\bar{C}_h = 0$, then (18) is still valid as the interface boundary condition.

With a little algebra it can be shown that

$$\frac{\partial}{\partial T} (RK_\omega PH_r) = R \left(K_\omega H_r \frac{\partial P}{\partial T} + P \frac{\partial H_r}{\partial T} \right) \tag{19}$$

so the form of (13) of interest is

$$-\frac{\partial \Psi s}{\partial S} - \Lambda \frac{2\nu}{\omega_1 + \omega_2} R \left(K_\omega H_r \frac{\partial P}{\partial T} + P \frac{\partial Hr}{\partial T} \right) = 0. \tag{20}$$

APPENDIX 2. Equations of Motion

In this appendix we obtain the equations of motion for the axial dynamics of a spool bearing. Consider an inertial frame located at the center of the journal's initial position. Let x_t be the displacement of the stator and let it have mass M. Let x_ω be the displacement of the rotor and presume it has mass m. Let F be the gas film force and f the external force, then

$$Md^2x_t/dt^2 = f - F \tag{21}$$

$$md^2x_\omega/dt^2 = F \tag{22}$$

combining (21) and (22) gives

$$d^2(x_t - x_\omega)/dt^2 = f/M - F(m + M)/mM \tag{23}$$

Under the assumption $M \gg m$, $m/(m + M) \cong m/M$, so (23) becomes

$$md^2(x_t - x_\omega)/dt^2 = mf/M - F \tag{24}$$

using the convention that c_o is the nominal thrust plate clearance, it is convenient to redefine

$$x_t - x_\omega = c_o - \epsilon \tag{25}$$

where ϵ is defined as the displacement of the rotor relative to the stator (which is the dimensional axial eccentricity) with the convention that ϵ is positive in the direction of increasing S which generally would be the direction of the positive spin axis. By definition the positive direction of S along the journal points to the positive thrust plate, so $h_{r\pm} = c_o \mp \epsilon$, where $h_{r\pm}$ is the $\pm$ thrust plate gap.

Let $f/M = a_e$, the external acceleration, then (24) and (25) give

$$-md^2\epsilon/dt^2 = ma_e - F \tag{26}$$

Let $\bar{\epsilon} = \epsilon/c_o$; in nondimensional form (26) is

$$d^2\bar{\epsilon}/dt^2 = (-a_e + F/m)/c_o\nu^2, \tag{27}$$

and it is further convenient to put (27) in system form

$$\begin{aligned} d\bar{\epsilon}_1/dT &= \bar{\epsilon}_2 \\ d\bar{\epsilon}_2/dT &= (-a_e + F/m)/c_o\nu^2 \end{aligned} \tag{28}$$

where $\bar{\varepsilon}_1 = \varepsilon/c_o$ and $\bar{\varepsilon}_2 = (d\varepsilon/dt)/c_o\nu$.

Different methods are used to integrate (28) depending on the truncation error of the scheme used to integrate the Reynolds equation.

APPENDIX 3. Spatial Difference Approximations

The spatial difference approximations to (20) are obtained by conventional divergence (or integral) methods. An arbitrary mesh is used with discontinuities in any bearing parameter only being allowed to occur at a mesh point. Mesh points in the direction of increasing S are enumerated by the index J. Define $\Delta S_J = S_{J+1} - S_J$, and define the fundamental interval $i(J)$ to be

$$i(J) = [S_J - .5\,\Delta S_{J-1},\ S_J + .5\,\Delta S_J] \qquad (29)$$

which has length $.5(\Delta S_{J-1} + \Delta S_J)$. Integrate (20) over $i(J)$ to obtain

$$\Psi_{S,J+.5} - \Psi_{S,J+} + \Psi_{S,J-} - \Psi_{S,J-.5} = -\int_{i(J)} \Lambda \frac{2\nu}{\omega_1 + \omega_2}\, R\left(K_\omega H_r \frac{\partial P}{\partial T} + P\frac{\partial H_r}{\partial T}\right) \qquad (30)$$

Since $\Psi_{S,J+} = \Psi_{S,J-}$ except at the chamfer, by (18) (30) becomes

$$\begin{aligned}\Psi_{S,J+.5} - \Psi_{S,J-.5} = &-\int \Lambda \frac{2\nu}{\omega_1 + \omega_2}\, R\left(K_\omega H_r \frac{\partial P}{\partial T} + P\frac{\partial H_r}{\partial T}\right) dS \\ &-\Lambda \frac{c_o}{r_o} \frac{2\nu}{\omega_1 + \omega_2}\, R_J \bar{C}_h \left(P\frac{\partial H_r}{\partial T} + \bar{C}_h \frac{\partial P}{\partial T}\right)\end{aligned} \qquad (31)$$

where the second term on the right appears only at the chamfer.

Define

$$\begin{aligned} a &= [P H_r^3 K_1 R] \\ b &= [\Lambda_\delta K_4 R^2 \cos\beta\ P] \\ g &= \Lambda \frac{2\nu}{\omega_1 + \omega_2} [R\ K_\omega H_r] \\ c &= \Lambda \frac{2\nu}{\omega_1 + \omega_2} [RP\ \partial H_r / \partial T] \\ \Delta_J P &= (P_{J+1} - P_J)/\Delta S_J \end{aligned} \qquad (32)$$

The basic approximation to be used to (31) is

$$
\begin{aligned}
& a_{J+.5}\Delta_J P - b_{J+.5} - a_{J-.5}\Delta_{J-1} P + b_{J-.5} \\
& = .5\left(\Delta S_J\, g_{J+} + \Delta S_{J-1}\, g_{J-}\right) \frac{P_J^{n+1} - P_J^{n}}{\Delta T} + .5\left(\Delta S_J c_{J+} + \Delta S_{J-1} c_{J-}\right) \\
& + \Lambda \frac{c_o}{r_o} \frac{2\nu}{\omega_1 + \omega_2}\, R_j\, \bar{c}_h \left(P_J\, [\partial H_{r,J+}/\partial T + \partial H_{r,J-}/\partial T] + \bar{c}_h \frac{P_J^{n+1} - P_J^{n}}{\Delta T}\right)
\end{aligned} \tag{33}
$$

where superscript n refers to the n-th time step. Subscript J refers to the J-th spatial mesh point. All quantities defined at the spatial half step that cannot be analytically directly determined are obtained by linear interpolation, e.g. $P_{J+.5} = .5(P_J + P_{J+1})$. Quantities such as g_{J+} and g_{J-} are respectively the right and left limits at the J-th mesh point of g. The replacement of $\partial H_r/\partial T$ by $\partial H_{r,J+}/\partial T + \partial H_{r,J-}/\partial T$ is valid since one term or the other is 0 at the chamfer.

APPENDIX 4. Geometry of Spool Bearing

The pertinent parameters for the spool bearing examples given are summarized in Table 4.

TABLE 4. SPOOL BEARING PARAMETERS

Parameter	Thrust	Journal
α	.5	.5
β (degrees)	166	30
δ (in.)	$136(10)^{-6}$	$136(10)^{-6}$
h_r (in.)	$90(10)^{-6}$	$90(10)^{-6}$
$\overline{Y}$	.65	.40
r_o (in.)	.52	-
r_i (in.)	.23	-
L (in.)	-	1.8
r_j (in.)	-	.23
ω_2 (RPM)	0	24,000
ω_1 (RPM)	24,000	0

Other quantities are p_a = 29.4 lb./in.^{2}, μ = 3.02 $(10)^{-9}$ lb. sec/in.^{2}, and m = 49 gm.

NOMENCLATURE

Upper Case English

$\bar{C}_h$	=	c_h/c_o, nondimensional chamfer height
F	=	gas film force in axial direction (lb.)
H	=	nondimensaional bearing gap for plain journal bearing
H_r	=	h_r/c_o, nondimensional bearing gap
$H_{r\pm}$	=	H_r at positive or negative thrust plate
J	=	subscript indicating J-th spatial mesh point
J±	=	subscript indicating right or left limit at J-th mesh point
K	=	$(U^2 + V^2)^{1/2}$, total bearing stiffness (lb./in.)
K_1	=	Whipple coefficient [See (15)]
K_4	=	"
K_ω	=	"
L	=	length of journal bearing (in.)
M	=	mass of stator (lb. sec.^{2}/in.)
P	=	p/p_a, nondimensional pressure
R	=	r/r_o, nondimensional radial distance from axis of symmetry.

S	=	s/r_o, nondimensional meridianal coordinate
T	=	νt, nondimensional time
T'	=	$T/(2\pi/288)$, abscissa of figures
U	=	in-phase bearing stiffness
V	=	out-of-phase bearing stiffness
V_o	=	constant term of $V = V_o + V_1/N^*$
V_1	=	coefficient of linear term of $V = V_o + V_1/N^*$
$\overline{Y}$	=	ratio of grooved region to total bearing extent in the meridianal direction

Lower Case English

a	=	coefficient for difference approximation [See (32)]
a_e	=	f/M, external acceleration (in./sec.^{2})
a_i	=	Fourier series coefficient [See (5)]
a_1	=	coefficient of cos(T) term [See (5)]
b	=	coefficient for difference approximation [See (32)]
b_i	=	Fourier series coefficient [See (5)]
b_1	=	coefficient of sin(T) term [See (5)]

c	=	coefficient for difference approximation [See (32)]
c_o	=	nominal clearance used to nondimensionalize quantities (in.)
c_h	=	chamfer height (in.)
f	=	external force on bearing (lb.)
g	=	coefficient for difference approximation [See (32)]
h_r	=	bearing clearance (in.)
$h_{r\pm}$	=	h_r at positive or negative thrust plate
$i(J)$	=	mesh interval from midpoint to midpoint [See (29)]
m	=	rotor mass (lb. sec.^{2}/in.)
n	=	superscript designating time [e.g., $P^n = P(n\Delta T)$]
p	=	pressure (lb./in.^{2})
p_a	=	ambient pressure (lb./in.^{2})
r	=	radial distance from axis of symmetry (in.).
r_o	=	outer radius of thrust plate (in.)
r_i	=	inner radius of thrust plate (in.)
r_j	=	journal radius (in.)
s	=	meridianal coordinate (in.)
t	=	time (sec.)

x_t = displacement of stator (in.)

x_ω = displacement of rotor (in.)

Upper Case Greek

Γ = $(h_r + \delta)/h_r$, groove depth ratio

Δ_J = forward difference with respect to S, e.g., $\Delta_J P = (P_{J+1} - P_j)/\Delta S_J$

ΔS_J = mesh spacing at J-th mesh point, $\Delta S_J = S_{J+1} - S_J$

ΔT = nondimensional time step

Λ = compressibility number [See (15)]

Λ_δ = Whipple coefficient [See (15)]

Ψ_S = nondimensional mass flux [See (14)]

$\Psi_{S|in}$ = nondimensional mass flux flowing into chamfer

$\Psi_{S|out}$ = nondimensional mass flux flowing out of chamfer

Lower Class Greek

α = ratio of groove width to sum of groove and ridge width

β = spiral groove angle

δ = groove depth (in.)

ϵ	=	dimensional axial eccentricity (in.) [See (25)]
$\bar{\epsilon}$	=	ϵ/c_0, nondimensional eccentricity
$\bar{\epsilon}_1$	=	ϵ/c_0, nondimensional eccentricity (Same as ϵ)
$\bar{\epsilon}_2$	=	$(d\epsilon/dt)/c_0 v$, nondimensional eccentricity velocity
μ	=	viscosity (lb.sec./in.^{2})
ν	=	frequency (radians/sec.)
ϕ	=	arctan (-V/U), phase angle (radians)
ω_1	=	smooth surface rotational speed (radians/sec.)
ω_2	=	grooved surface rotational speed (radians/sec.)

<u>Other</u>

$\pm$	=	subscript used to denote positive and negative thrust plate or when used as $J\pm$ indicates right or left limit at J-th mesh point

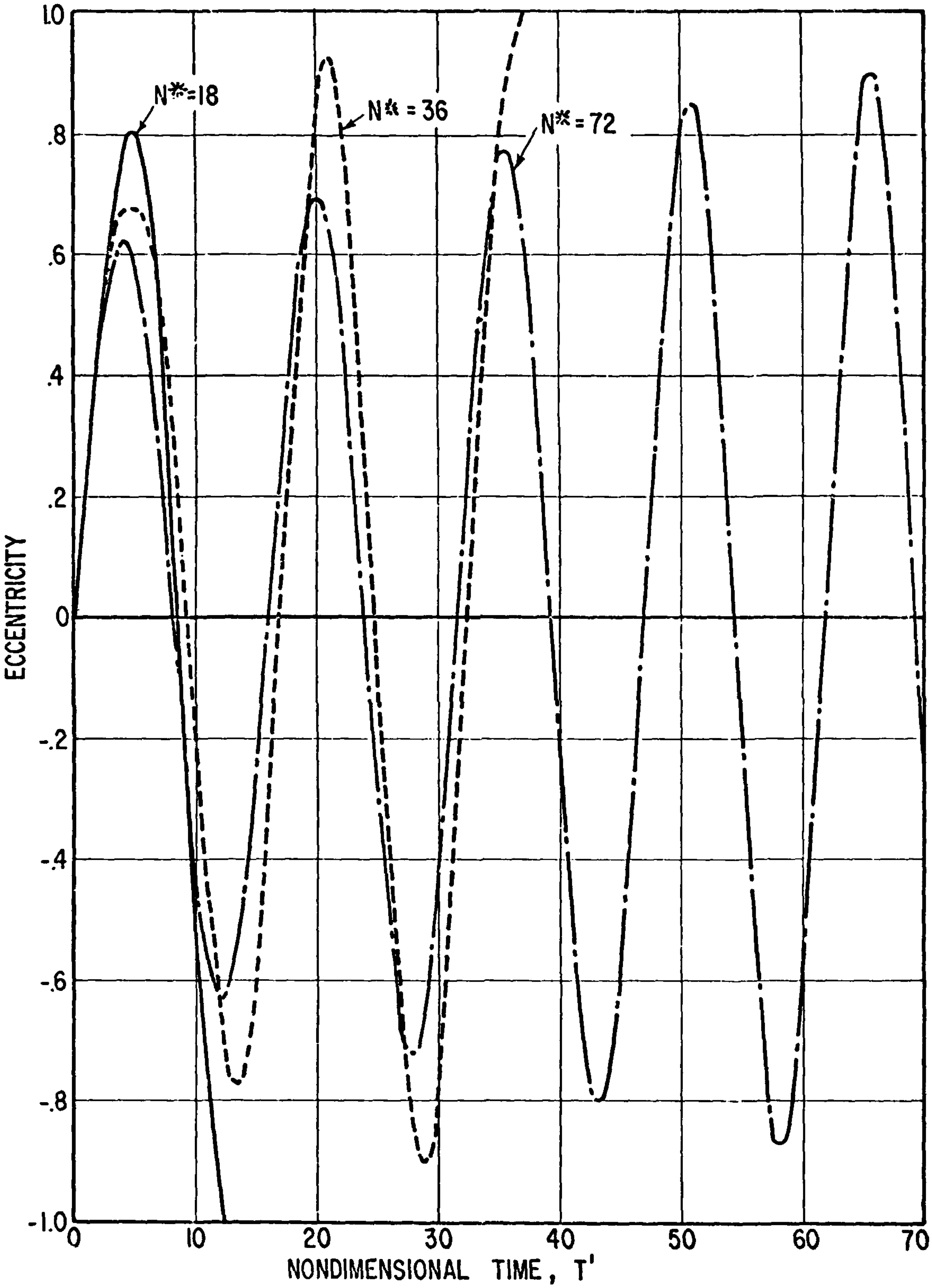

Figure 1 - Implicit Scheme Axial Dynamics for Differing Time Steps

MTI-11612

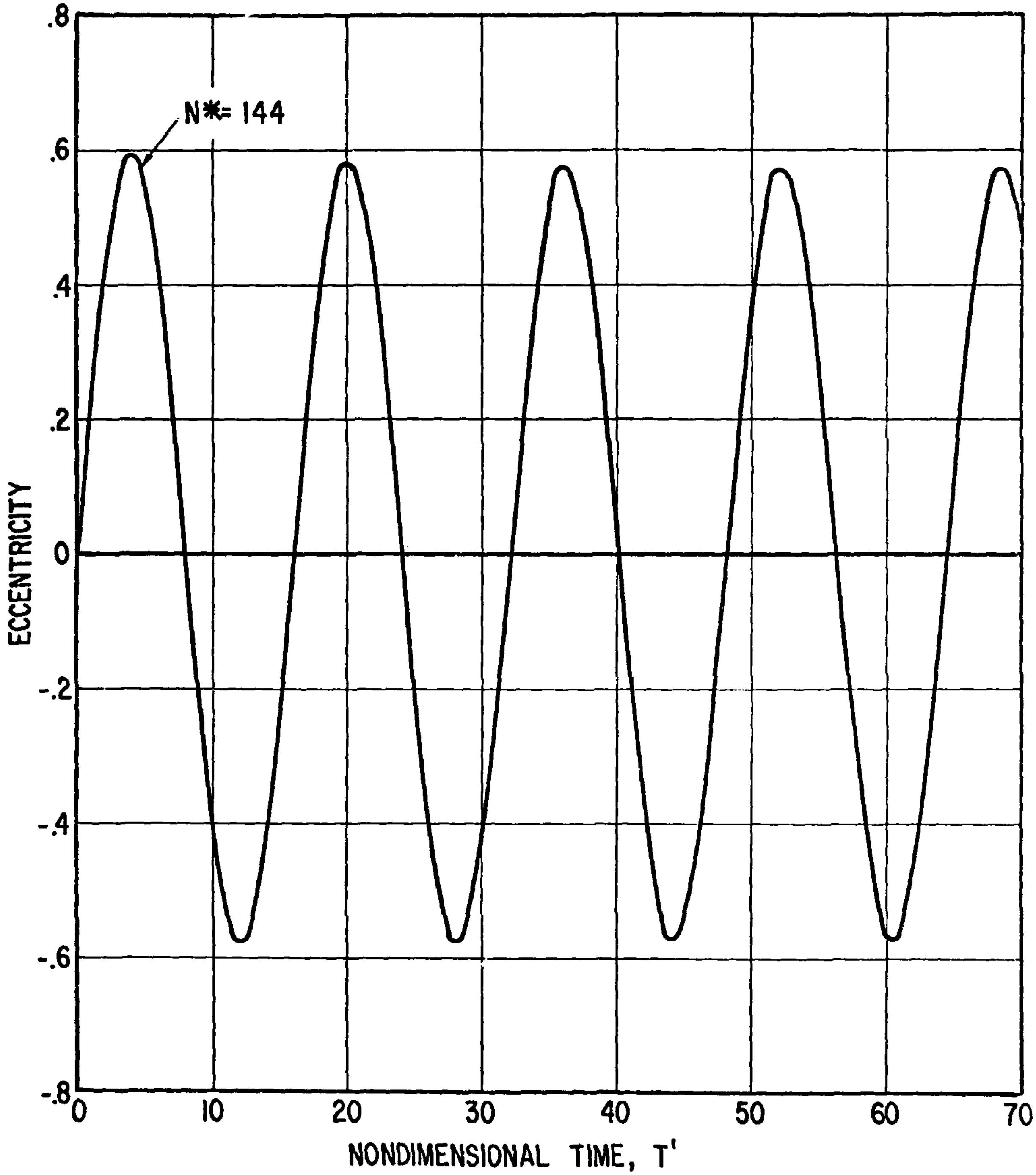

Figure 2 - Implicit Scheme Axial Dynamics for Very Fine Time Step

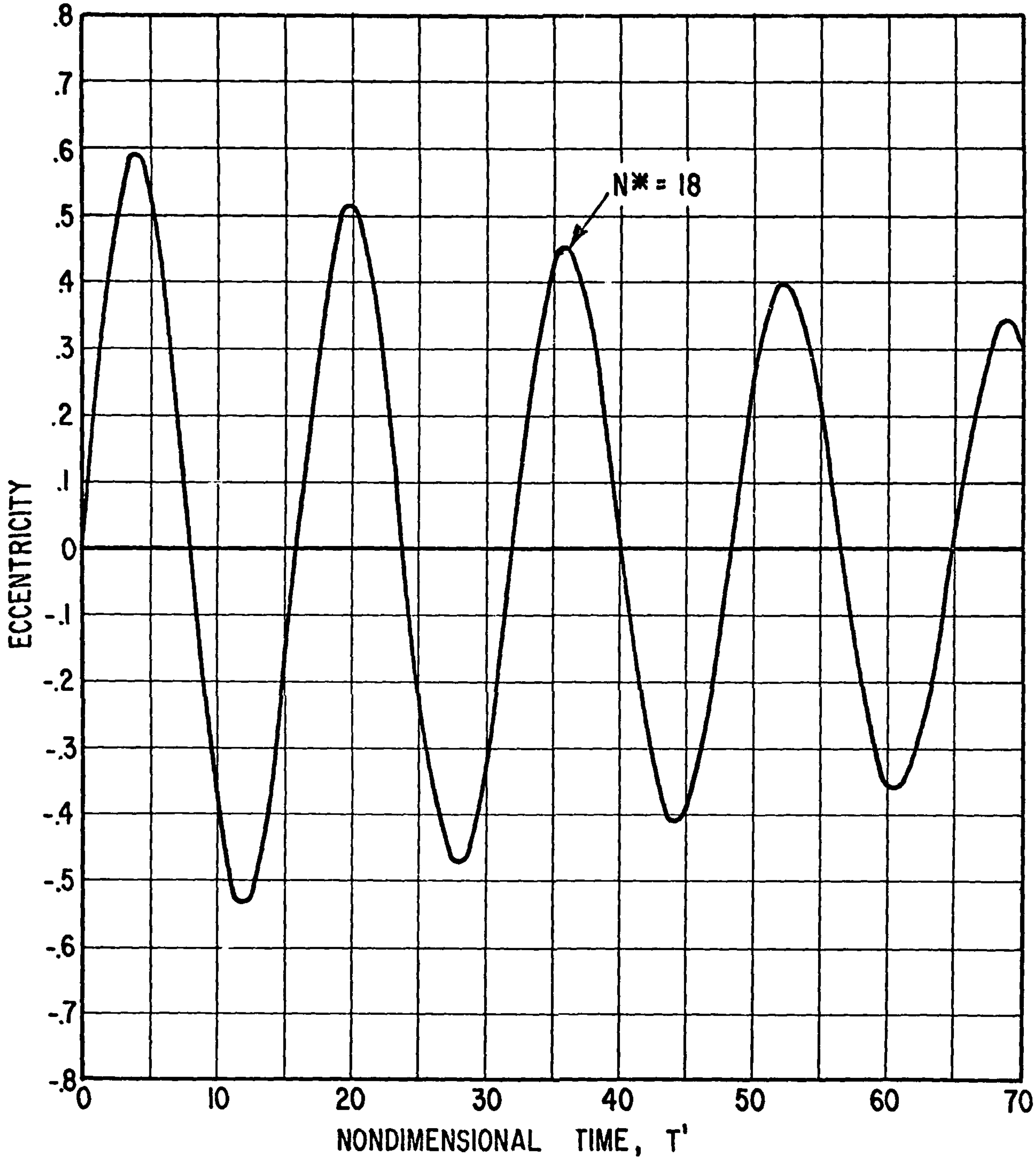

Figure 3 - Extrapolated Crank-Nicolson Scheme at Coarse Time Step